Bull. Chem. Soc. Ethiop. **2024**, 38(5), 1429-1437.
DOI: https://dx.doi.org/10.4314/bcse.v38i5.18

ISSN 1011-3924
Printed in Ethiopia
Online ISSN 1726-801X

LIQUID-COMBUSTION SYNTHESIS OF SPINEL $LiMn_2O_4$ CATHODE MATERIAL FOR ENHANCED ELECTROCHEMICAL PERFORMANCE LITHIUM-ION BATTERIES

Yu Sun[1], Chaofan Li[2*], Hongcheng Gao[1], Jiaming Li[1] and Jiabin Hao[1*]

[1.] Department of Chemical Engineering, Hebei Petroleum University of Technology, Chengde 067000, China
[2.] Department of Automotive Engineering, Hebei Petroleum University of Technology, Chengde 067000, China

(Received November 3, 2023; Revised February 19, 2024; Accepted May 20, 2024)

ABSTRACT. A cubic spinel $LiMn_2O_4$ cathode material with nanoscale was synthesized *via* a facile liquid-combustion method at 600, 750 and 850 °C. The crystal structure and surface morphology of $LiMn_2O_4$ electrodes have been characterized by using X-ray diffraction (XRD), scanning electron microscopy (SEM) and transmission electron microscopy (TEM) technique. The samples have an average diameter of 200 nm with an octahedral structure with high crystallinity. Benefiting from the excellent structure, the sample prepared at 750 °C delivers the highest first discharge capacity of 115.3 $mAh \cdot g^{-1}$ with remaining 101.5 $mAh \cdot g^{-1}$ after 400 cycles at 1 C. Moreover, it exhibits a good cycling performance at 55 °C, still had the capacity of 105.4 $mAh \cdot g^{-1}$ with a capacity retention of 71.2% following 282 cycles. The facilely synthesized octahedral $LiMn_2O_4$ provides a practical application strategy for lithium-ion batteries.

KEY WORDS: Spinel $LiMn_2O_4$, Liquid-combustion method, Lithium-ion batteries

INTRODUCTION

Nowadays, rechargeable lithium-ion batteries (LIBs) have promoted renewable energy development and achieved impressive success in application fields such as essential energy storage devices as well as electric vehicles (EVs) and hybrid electric vehicles (HEVs). The electrochemical performance of LIBs is mainly determined by the cathode materials [1, 2]. Considering the high abundance, environmental friendliness, low cost, fine safety and abundant manganese resources, spinel $LiMn_2O_4$ has been intensively studied as one of the most promising LIBs cathode materials. In particular, spinel $LiMn_2O_4$ has high operating voltage and a robust structure with a three-dimensional network, which can provide excellent Li^+/electron transport channels during Li^+ insert/extraction and high operation potential [3-5]. However, it still suffers from structural transformation and capacity fading caused by Mn dissolution, the Jahn-Teller effect and electrolyte decomposition [4, 5]. These problems also severally limit its large-scale application.

The conventional solid-state reaction is widely used to prepare $LiMn_2O_4$ materials. However, the drawbacks of this method, such as long calcination time, slow reaction kinetics and impure phase product have constrained its practical application [6-10]. Therefore, various researches and approaches have been studied to overcome above drawbacks and enhance performance of $LiMn_2O_4$ materials, such as liquid state reactions, sol–gel method, Pechini method, spray drying method and combustion synthesis [11-23]. Zhao et al. used the sol-gel technology to prepare the Er-doped $LiMn_2O_4$ cathode materials. This sample delivered a reversible capacity of 130.2 $mAh \cdot g^{-1}$ with an excellent retention of 95.2% after 100 cycles at 0.5 C [11]. Yang and co-workers synthesized a two-stage calcination Co-doped $LiMn_2O_4$ sample which revealed an initial specific

*Corresponding authors. E-mail: CfLi_HEBPU@163.com; jiajooy@163.com

discharge capacity of 121.9 $mAh \cdot g^{-1}$ at 0.2 C and a capacity retention of 80.6% after 60 cycles [19]. Palaniyandy and co-workers successfully prepared the renovated spinel $LiMn_2O_4$ material, and it exhibited a better cycling stability with the discharge capacity of 56 $mAh \cdot g^{-1}$ after 500 cycles at 1 C [20]. Huang and co-workers adopted a carbohydrate-assisted combustion method synthesized $LiMn_2O_4$ spinel that showed a good cycling stability of 92% capacity retention after 100 charge/discharge cycles [21]. Yao and co-workers prepared the $LiMn_2O_4$ cathode material directly from the leaching solution of waste LIBs, which avoided the complex separation process [22]. Nakajima and co-workers used calorimetry to measure the interfacial energies of $LiMn_2O_4$ nanoparticles for the first time, and they found that Sc-doped $LiMn_2O_4$ has lower surface energy significantly than undoped $LiMn_2O_4$ likely because of the dopant's segregation to grain boundaries affecting the distribution of Li^+ across the material [23].

In this work, we demonstrate a liquid-state combustion synthesis to prepare spinel $LiMn_2O_4$ cathode material, in which a solution mixture of aqueous metal salts and nitric acid used as the fuel generated a self-combustion reaction at temperature from 600 to 850 ℃ in air atmosphere. Based on this method, the $LiMn_2O_4$ samples showed not only pure single-phase spinel product with high crystallinity but also high cell-cycling and electrochemical performance. Specially, it provides an efficient method with facile process, time-consuming and uniform distribution particles for spinel $LiMn_2O_4$ cathode material in lithium-ion batteries.

EXPERIMENTAL

Spinel $LiMn_2O_4$ preparation

The spinel $LiMn_2O_4$ cathode material was prepared by using a liquid-state combustion method. In a typical synthesis required for preparing 3 g $LiMn_2O_4$ target product, the reactor consisting of $LiNO_3$ (AR, Aladdin, 99.0%) and $Mn(CH_3COO)_2 \cdot 4H_2O$ (AR, Aladdin, 99.0%) were accurately weighted according to a molar ratio of Li:Mn = 1:2 and dissolved in the nitric acid with a concentration of 9 mol/L in a crucible. The mixture was heated in an oven at 100 ℃ to form a homogenous solution. To obtain spinel $LiMn_2O_4$, the as-prepared solutions were calcined at 600 ℃ (LMO-T600), 750 ℃ (LMO-T750) and 850 ℃ (LMO-T850) for 3 h, respectively. Through an autoxidative combustion reaction, the products were cooled off to room temperature and grounded to form spinel $LiMn_2O_4$ samples.

Characterization of materials

X-ray diffraction (XRD) was performed on a Bruker D8 Advance diffractometer with Cu $K\alpha$ radiation, and 2θ data range collected from 10° to 70°. The morphology and lattice structure of the samples were characterized by field emission scanning electron microscope (FE-SEM, NOVA NANOSEM 450, America FEI) and transmission electron microscope (TEM, JEM-2100).

Electrochemical measurements

The electrochemical properties of the samples were carried out using CR2025 coin-type cells assembled in a glove box (MBraun, Germany) filled with high purity argon gas. The cathode slurry was fabricated by ball-mill mixing the active material, polyvinylidene fluoride (PVDF) and carbon black with a weight ratio of 8:1:1 dissolved in N-methyl-2-pyrrolidone (NMP) solvent, and the weight of active material in each electrode was about 2 mg. Then, the slurry was homogeneously coated onto an aluminum foil current collector using doctor-blade technique and dried in an oven, and then the spinel $LiMn_2O_4$ cathode material with the mass loading of about 1.0 mg/cm^2 was obtained. Finally, all as-prepared cathode disks were stored a vacuum drying

oven at 120 ℃ for 8-12 h. 1 M $LiPF_6$ in EC/DMC (1:1 in volume) and Celgard 2320-type membrane were used as anode, electrolyte and separator, respectively. The cells were cycled by a galvanostatical charge-discharge tests were measured by the Land electric test system CT2001A in the voltage from 3.0 to 4.5 V (versus Li^+/Li). Cyclic voltammetry (CV) and electrochemical impedance spectroscopy (EIS) were tested by an electrochemical workstation of CHI660D between 3.6 and 4.5 V.

RESULTS AND DISCUSSION

XRD studies

XRD patterns of LMO-T600, LMO-T750 and LMO-T850 samples are shown in Figure 1. The XRD spectra of all samples could be indexed to the standard PDF card No. 35-0782. The diffraction peaks of (111), (311), (222), (400), (331), (511), (441) and (531) correspond to a single-phase of spinel $LiMn_2O_4$ with *Fd*-3*m* space group. As shown in this result, the LMO-T600 electrode shows impurities peaks of Mn_3O_4, which may be due to the lower calcination temperature resulting in poor crystallization. Furthermore, compared to the T850 sample, the LMO-T750 electrode shows sharper peaks and larger peak area, indicating a better crystallinity. Considering of the crystallinity property, the optimal temperature has been determined as 750-850 ℃.

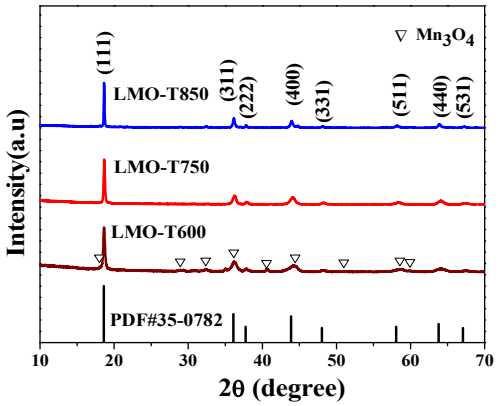

Figure 1. XRD diagram of LMO-T600, LMO-T750 and LMO-T850 samples.

SEM analysis

The morphology images and size distribution of the $LiMn_2O_4$ samples calcined at different temperature are shown in Figure 2. The LMO-T600 sample has random particle morphology with the arrangement of particles in aggregates/agglomerations, which will greatly decrease specific capacity. With an increase in the calcination temperature at 750 ℃, the LMO-T750 samples became more uniform and maintain a narrow distribution with particles diameter of about 200 nm. When the calcination temperature was as high as 850 ℃, The LMO-T850 samples showed heterogeneous particle size dispersion with diameters of larger particles of about 300 nm and less than 100 nm, which could be due to severe sintering effect [1, 13]. On the basis of SEM images, the LMO-T750 samples showed nanosized particles with high surface area and high crystallinity, which may exhibit better electrochemical properties and rate performance. To obtain more insights in the microstructure, the LMO-T750 material was carefully examined by high-resolution

transmission electron microscope (HRTEM), shown in Figure 2(d) and (e). As seen, the sample showed as octahedrons and a well-defined lattice fringe of 0.48 nm, which is in accordance with the (111) plane of the spinel $LiMn_2O_4$ [3, 4, 28].

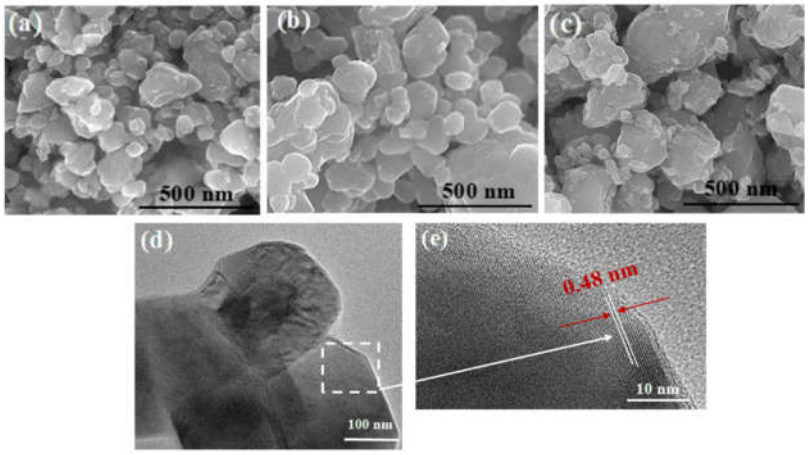

Figure 2.SEM images of $LiMn_2O_4$ samples of (a) LMO-T600, (b) LMO-T750, (c) LMO-T850, (d) TEM and (e) HRTEM images of $LiMn_2O_4$ sample of LMO- T750.

Electrochemical performance

To evaluate the electrochemical performance of the LMO-T600, LMO-T750 and LMO-T850 samples, a galvanostatic charge/discharge test was conducted in a voltage range of 3.0-4.5 V. All cycling performances of the samples at 1 C are depicted in Figure 3. The initial and 400th discharge specific capacities and capacity retentions of the samples are summarized in Table 1. As shown Figure 3(a), the first discharge capacity is 101.7, 112.1 $mAh \cdot g^{-1}$ at 1 C with a capacity retention of 72.2% and 82.3% after 400 cycles for the LMO-T600 and LMO-T850 samples, respectively. The LMO-T750 electrode delivers a first cycle discharge specific capacity of is 115.3 $mAh \cdot g^{-1}$ at 1 C and 101.5 $mAh \cdot g^{-1}$ after 400 cycles, corresponding to a capacity retention of 88.0%, which probably is due to the reduced Mn dissolution in the truncated octahedron and decrease of Li^+ loss inside the lattice [5]. Figure 3(b) shows the first cycle of discharge curves for the samples at current density of 1 C. Obviously, the samples exhibit two plateaus at around 3.9 and 4.1 V, corresponding to the two-step oxidation/reduction reaction process for the spinel $LiMn_2O_4$ [24].

In addition, we compared the cycling performance of the $LiMn_2O_4$ and Co-doped $LiMn_2O_4$ samples, as shown in Table 2. It can be found that the LMO-750 displays good cycling performance. This result suggests that the facile liquid-combustion method can effectively improve cycle stability of lithium-ion batteries.

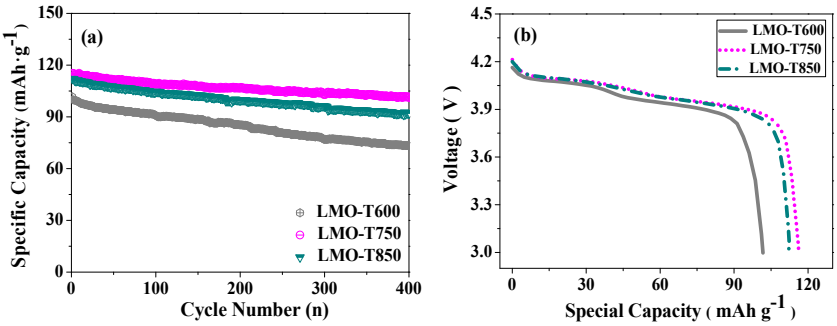

Figure 3. Electrochemical performances of LMO-T600, LMO-T750 and LMO-T850: (a) cycling performance curves at 1 C and (b) first charge-discharge curve at 1 C.

Table 1. Discharge specific capacity and capacity retention rate of LMO-T600, LMO-T750 and LMO-T850 samples at room temperature.

Samples	Initial capacity ($mAh \cdot g^{-1}$)	400^{th} capacity ($mAh \cdot g^{-1}$)	Capacity retentions (%)
LMO-T600	101.7	73.4	72.2
LMO-T750	115.3	101.5	88.0
LMO-T850	112.1	92.2	82.3

Table 2. Comparison of the $LiMn_2O_4$ and Co-doped $LiMn_2O_4$ samples described in the references including this work.

Samples	Synthesis Method	Initial capacity and Capacity Retention	Ref.
$LiMn_2O_4$	Sol-gel method	137 $mAh \cdot g^{-1}$, 67.8% after 100 cycles at 0.5 C (25 °C)	[11]
$LiCo_{0.04}Mn_{1.96}O_4$	Liquid-phase fameless combustion	121.9 $mAh \cdot g^{-1}$, 80.6% after 60 cycles at 0.2 C (25 °C)	[19]
$LiMn_2O_4$	A facile segregation process	About 56 $mAh \cdot g^{-1}$, about 100% after 500cycles at 1.0 C (25 °C)	[20]
$LiMn_2O_4$	Sol-gel method	125 $mAh \cdot g^{-1}$, about 92% after 100cycles at 1.0 C (25 °C)	[21]
$LiMn_2O_4$	Liquid-combustion method	115.3 $mAh \cdot g^{-1}$, about 88% after 400 cycles at 1.0 C (25 °C)	This work

Figure 4(a) displays the rate performance of the LMO-T600 and LMO-T750 cathodes at charge/discharge current densities ranging from 0.5 C to 10 C. Apparently, the discharge specific capacities of both of samples gradually decrease with increasing of charge/discharge rate, which is due to the electrochemical polarization in the Li^+ diffusion process [25]. The LMO-T750 electrode delivers an average specific capacity of 110.1, 104.4, 96.5, 89.6 and 72.1 $mAh \cdot g^{-1}$, respectively, in contrast to 102.7, 95.8, 85.1, 68.8 and 48.3 $mAh \cdot g^{-1}$ for the LMO-T600 electrode. While the current density returns back to 0.5 C again, the reversible capacity of 97.7% of the original capacity for the LMO-T750 electrode, proving a superior reversibility. The good high-rate capability is governed not only by the size of crystallites but also by the perfectness of crystals, which is well consistent with the analytical results of XRD patterns and SEM analysis. The high-temperature cycle performance of the LMO-T600 and LMO-T750 samples at 55 °C is shown in Figure 4(b). The LMO-T750 electrode delivers an initial discharge capacity of 105.4 $mAh \cdot g^{-1}$, which is higher than that of 92.3 $mAh \cdot g^{-1}$ for the LMO-T600 sample. Therefore, the

results indicate the optimized calcination temperature could strongly enhance the cycle performance and rate performance.

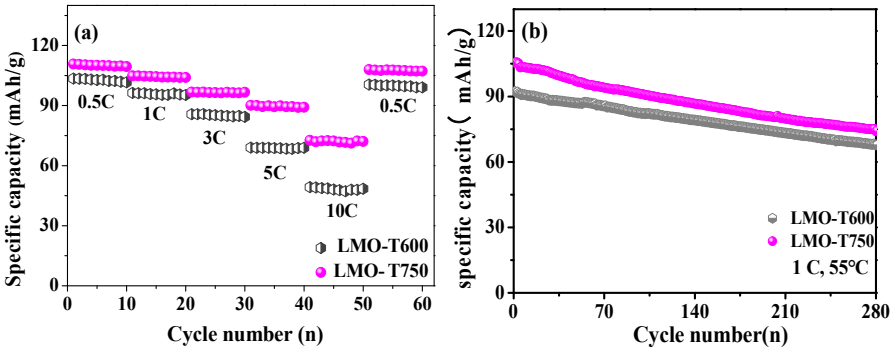

Figure 4. Electrochemical performances of $LiMn_2O_4$ samples of T600 and T750: (a) rate capability at 0.5-10 C and (b) cycling performance curves at 1 C, 55 ℃.

Cyclic voltammogram

To analyze the phase transformation process, cyclic voltammetry curves (CV) of the samples in voltage range of 3.6-4.5 V with a scanning rate of 0.05 mV/s are provided in Figure 5(a) and (b). As seen, all of the samples display a couple of distinct redox peaks, indicating the two-stage Li^+ insertion/extraction process of the spinel $LiMn_2O_4$ cathode material, which is consistent with the two-plateaus in the charge/discharge profiles [27, 29]. Figure 5(a) shows that the area of the LMO-T600 cathode is obviously smaller than that of the other two electrodes with similar peak areas, corresponding to the current densities of the cycle curves. After 100 cycles, the LMO-T750 electrode shows a large peak area and sharp peak shown in Figure 5(b), indicating a higher discharge capacity and a faster insertion/extraction kinetics of Li^+ ions than the other samples [26].

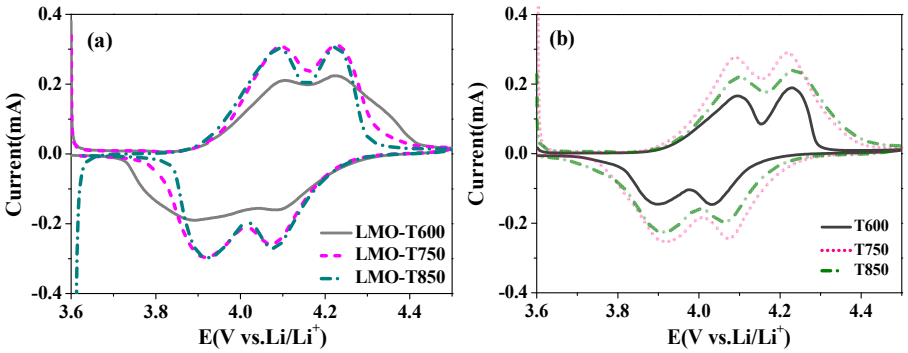

Figure 5. Cyclic voltammetry curves of LMO-T600, LMO-T750 and LMO-T850 after the (a) 1st and (b) 100th.

Electrochemical impedance spectroscopy

To further investigate the electrochemical mechanism and inner impedance for the samples, the electrochemical impedance spectroscopy (EIS) and the fitting equivalent circuit diagram is studied, as shown in Figure 6. Where, the ohmic resistance (R_s) represents the resistance of electrolyte and solution inner the cell, corresponding to one semicircle in the high frequency region. Besides, the charge transfer resistance (R_{ct}) is related to the electrochemical performance of the cells, which is located in the medium region. In addition, the CPE responds the double-layer capacitor and W is the Warburg impedance in the EIS [27]. Table 3 depicts the R_s and R_{ct} values obtained from the fitting equivalent circuit diagram. As shown in the Figure, all samples have similar R_s values. The value of the R_{ct} (161.3 Ω) of the LMO-T750 electrode is less than that of the LMO-T600 (268.5 Ω) and LMO-T850 (279 Ω) samples, indicating a lower resistance for charge transfer during cycling process, resulting in a better electrochemical performance and rate performance.

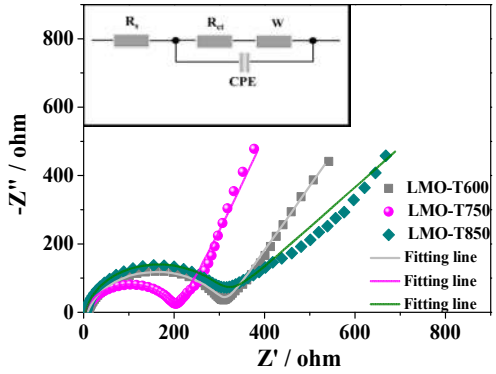

Figure 6. The Nyquist plots and the equivalent circuit of LMO-T600, LMO-T750 and LMO-T850.

Table 3. The fitting valves of the equivalent circuit.

Samples	R_s /Ω	R_{ct} /Ω
LMO-T600	8.71	268.5
LMO-T750	7.42	161.3
LMO-T850	6.36	297.0

CONCLUSION

We have prepared the spinel $LiMn_2O_4$ cathode materials by a facile liquid-state combustion synthesis and then qualitatively and quantitatively invested the property and electrochemical performance in the lithium-ion batteries, including the changes in the crystal structure, Li^+ ions diffusion kinetics, phase transformation process, cycling performances, etc. The truncated morphology of the LMO-T750 sample caused by the solution combustion method and then resulted in an increase of the discharge capacity. As a result, the LMO-T750 electrode showed 88.0% capacity retention with an initial discharge specific capacity of is 115.3 $mAh \cdot g^{-1}$, which was much higher than that of the LMO-T600 and LMO-T850 samples. We also observed that the minimal Mn dissolution in the LMO-T750 electrode induced a high current rate and high-temperature cycle performance. Moreover, the lower electrochemical impedance of the LMO-T750 electrode accelerated the Li^+ insertion/extraction process, indicating a better Li^+ diffusion

capability in the lithium-ion batteries. Our study suggested that this strategy may be an effective novel approach for improving the electrochemical performance and properties of lithium-ion batteries.

ACKNOWLEDGEMENT

This work is supported by Science Research Project of Hebei Education Department, China (QN2023068)

REFERENCES

1. Zhu, C.; Nobuta, A.; Saito, G.; Nakatsugawa, I.; Akiyama, T. Solution combustion synthesis of $LiMn_2O_4$ fine powders for lithium-ion batteries. *Adv. Powder Technol*. **2014**, 25, 342-347.
2. Potapenko, A.-V.; Kirillov, S.-A. Lithium manganese spinel materials for high-rate electrochemical applications. *J. Energy Chem*. **2014**, 23, 543-558.
3. Warburton, R.-E.; Iddir, H.; Curtiss, L.-A.; Greeley, J. Thermodynamic stability of low- and high-index spinel $LiMn_2O_4$ surface terminations. *ACS Appl. Mater. Int.* **2016**, 8, 11108-11121.
4. Nakajima, K.; Souza, F.-L.; Freitas, A.-L.-M, Thron, A.; Castro, R.-H.-R. Improving thermodynamic stability of nano-$LiMn_2O_4$ for Li-ion battery cathode. *Chem. Mater.* **2021**, 33, 3915-3925.
5. Gao, H.; Yan, Q.; Xu, P.; Liu, H.; Luo, J.; Cheng, Z. Efficient direct recycling of degraded $LiMn_2O_4$ cathodes by one-step hydrothermal relithiation. *ACS Appl. Mater. Int.* **2020**, 12, 51546-51554.
6. Yang, Z.; Huang, H.; Lin, F. Sustainable electric vehicle batteries for a sustainable world: Perspectives on battery cathodes, environment, supply chain, manufacturing, life cycle, and policy. *Adv Energy Mater.* **2022**, 12, 2200383.
7. Yu, F.-D.; Wang, Z.-B.; Chen, F.; Wu, J.; Zhang, X. G.; Gu, D.M. Crystal structure and multicomponent effects in $Li_{1+x}Mn_{2-x-y}Al_yO_4$ cathode materials for Li-ion batteries. *J. Power Sources* **2014**, 262, 104-111.
8. Jiang, C.; Tang, Z.; Wang, S.; Zhang, Z.-T.-A. truncated octahedral spinel $LiMn_2O_4$ as high-performance cathode material for ultrafast and long-life lithium-ion batteries. *J. Power Sources* **2017**, 357, 144-148.
9. Zhang, W.; Zhao, Z.; Lei, Y.; Xing, J.; Cao, X.-M.-A. Facile and eco-friendly approach to synthesis of spinel $LiMn_2O_4$ with high electrochemical performance. *Int. J. Electrochem Sci.* **2020**, 15, 6188-6197.
10. Uribe-Grajales, L.-M.; Vásquez-Arroyave, F.-A.; Thomas, J.-E.; Calderón-Gutiérrez, J.-A. Evaluation of the effect of the synthesis method on the performance of manganese spinel as cathode material in lithium-ion batteries. *Revista Facultad de Ingeniería Universidad de Antioquia* **2018** (87), 41-49.
11. Zhao, H.; Bai, X.; Wang, J.; Li, D.-D.; Li, B.; Wang, Y.-S.; Dong, L.; Liu, B.-B.; Komarneni, S. Enhanced cycling stability through erbium doping of $LiMn_2O_4$ cathode material synthesized by sol-gel technique. *Materials* **2018**, 11, 1558.
12. Xu, W.; Li, Q.; Guo, J.-M.; Bai, H.-L.; Su, C.-W.; Ruan, R.-S.; Peng, J.-H. Electrochemical evaluation of $LiZn_xMn_{2-x}O_4$ ($x \leq 0.10$) cathode material synthesized by solution combustion method. *Ceram. Int.* **2016**, 42, 5693-5698.
13. Liu, Q.; Zhong, L.; Guo, Y.; Xiang, M.-W.; Su C.-W.; Ning, P.; Guo, J.-M. Facile flameless combustion synthesis of high-performance boron-doped $LiMn_2O_4$ cathode with a truncated octahedra. *J. Alloy Compd.* **2021**, 874, 159912.
14. Chen, P.; Wu, H.; Huang, S.; Zhang, Y. Template synthesis and lithium storage performances of hollow spherical $LiMn_2O_4$ cathode materials. *Ceram. Int.* **2016**, 42, 10498-10505.
15. Sharma, R.; Sharma, M.; Goswamy, J.-K. $LiMn_2O_{4-r}$GO/PANI nanocomposite as a cathode material for Li-Ion batteries. *J. Electrochem. Soc.* **2022**, 169, 083505.

16. Putra, T.-Y.-S.-P.; Yonemura, M.; Torii, S.; Ishigaki, T.; Kamiyama, T. Structure and electrochemical performance of the spinel- $LiMn_2O_4$ synthesized by mechanical alloying. *Solid State Ionics* **2014**, 262, 83-87.
17. Lin, Y.; Välikangas, J.; Sliz, R.; Molaiyan, P.; Hu, T.; Lassi, U. Optimized morphology and tuning the Mn^{3+} content of $LiNi_{0.5}Mn_{1.5}O_4$ cathode material for Li-ion batteries. *Materials* **2023**, 16, 3116.
18. Leong, V.-G.-H.; Hong, S.-S.; Castro, R.-H.-R. Improved electrochemical performance in Sc-doped nanocrystalline $LiMn_2O_4$. *Mater. Lett.* **2022**, 325, 132824.
19. Yang, F.; Huang, J.; Hao, J.; Li, Q.; Bai, H.; Su, C.; Guo, J.M. Characterization of spinel-type $LiCo_{0.04}Mn_{1.96}O_4$ prepared by liquid-phase famless combustion. *Int. J. Electrochem. Sci*. **2015**, 10, 4044-4052.
20. Palaniyandy, N.; Rambau, K.; Musyoka, N.; Ren, J.-A. Facile segregation process and restoration of $LiMn_2O_4$ cathode material from spent lithium-ion batteries. *J. Electrochem. Soc.* **2020**, 167, 090510.
21. Huang, W.; Wang, G.; Luo, C.; Xu, Y.; Chen, Y.; Wang, B.; Huang, J.; Kang, Y.; Wu, J.; Dravid, V.P.; Facchetti, A.; Marks, T.-J. Controllable growth of $LiMn_2O_4$ by carbohydrate-assisted combustion synthesis for high performance Li-ion batteries. *Nano Energy* **2019**, 64, 103936.
22. Yao, L.; Xi, Y.; Han, H.; Li, W.; Wang, C.; Feng, Y. $LiMn_2O_4$ prepared from waste lithium-ion batteries through sol-gel process. *J. Alloys Compd.* **2021**, 868, 159222.
23. Nakajima, K.; Souza, F.-L.; Freitas, A.-L.-M.; Thron, A.; Castro, R.-H.-R. Improving thermodynamic stability of nano-$LiMn_2O_4$ for Li-ion battery cathode. *Chem. Mater.* **2021**, 33, 3915-3925.
24. Sintering: Mechanisms of convention nanodensification and field assisted processes. *Springer Science & Business Media*, **2012**.
25. Bhuvaneswari, S.; Varadaraju, U.-V.; Gopalan, R.; Prakash, R. Structural stability and superior electrochemical performance of Sc-doped $LiMn_2O_4$ spinel as cathode for lithium-ion batteries. *Electrochim. Acta* **2019**, 301, 342-351.
26. Liu, H.; Li, M.; Xiang, M.; Guo, J.; Bai, H.; Bai, W.; Liu, X. Effects of crystal structure and plane orientation on lithium and nickel co-doped spinel lithium manganese oxide for long cycle life lithium-ion batteries. *J. Colloid Interf. Sci*. **2021**, 585, 729-739.
27. Liu, J.; Li, G.; Bai, H.; Shao, M.; Su, C.; Guo, J.; Liu, X.; Bai, W. Enhanced cycle and rate performances of Li $(Li_{0.05}Al_{0.05}Mn_{1.90})O_4$ cathode material prepared *via* a solution combustion method for lithium-ion batteries. *Solid State Ionics* **2017**, 307, 79-89.
28. Kalam, A.; Allami, S.-A.-S.; Al-Sehemi, A.-G.; Assiri, M.-A.; Yadav, P. Effect of stabilizer on optical band gap of ZnO and their performance in dye-sensitized solar cells. *Bull. Chem. Soc. Ethiop.* **2022**, 36, 209-222.
29. Emre, F.B. Preparation of voltammetric sensors for taurine detection from Cu(II)-loaded carbon materials. *Bull. Chem. Soc. Ethiop*. **2023**, 37, 1565-1576.